Article:

A Robust Controller for Multi Rotor UAVs

Omar A. Jasim[1], Sandor M. Veres[2],[*]

Department of Automatic Control and Systems Engineering, University of Sheffield, Amy Johnson Building, Mappin Street, S1 3JD, UK

Abstract

Unmanned aerial vehicles (UAVs) are safety-critical systems that often need to fly near buildings and over people under adverse wind conditions and hence require high manoeuvrability, accuracy, fast response abilities to ensure safety. Under extreme conditions, the dynamics of these systems are strongly nonlinear and are exposed to disturbances, which need a robust controller to keep the UAV and its environment safe. In this paper a novel robust nonlinear multi-rotor controller is introduced based on essential modifications of standard dynamic inversion control, which makes it insensitive to payload changes and also to large wind gusts. First a robust attitude controller is established, followed by lateral and vertical position control in a customary outer loop. The controllers take into account thrust limitations of the aircraft and theoretical proof is provided for robust performance. The control scheme is illustrated in simulation with a realistic nonlinear dynamical model of an aircraft that includes rotor dynamics and their speed limitations to show

---

[*]Corresponding author

[1]Ph.D. candidate, Department of Automatic Control and Systems Engineering, University of Sheffield; e-mail: oajasim1@sheffield.ac.uk

[2]Professor, Department of Automatic Control and Systems Engineering, University of Sheffield; e-mail: s.veres@sheffield.ac.uk

robustness. Lyapunov stability methods are used to prove the stability of the robust control system.

1. Introduction

There is an increasing requirement for small multi-rotor unmanned drones, under 20kg and under 400ft, to be safely operated over congested, urban areas for police and security work, building inspections, fire fighting and emergency needs, etc. Drones would often carry variable payloads (cameras, measurement devices, pick-up arms, etc.) while they could be exposed to gusts of winds or could collide with or be attacked by other craft or birds. Other causes of instability may be a temporary deterioration of actuator or processor functionality. Under such conditions, a drone's dynamical state may be easily pushed into unstable regions if controlled by off-the-shelf axis-by-axis PD/PID controllers, see this in [1, 2]. It is therefore imperative that when these drones operate semi-autonomously by an autopilot, they would need software that monitors their operational conditions and takes action if the limits of the controller performance are approached. Ultimately, semi-autonomous drones would need to decide for themselves, or they should advise the remote pilot, in order to seek safety and to possibly modify or cancel flight/mission objectives.

A wide variety of control methods have been proposed in the literature to control and stabilize a multi-rotor UAV. In [3], a now classic approach, a PID controller of the multi-rotor was proposed for regulating the position and

orientation of the aircraft. A combination of PID and gain scheduling control approach is presented in [4] to increase robustness. In [5], a cascaded linear PID model-based controller on SO(3) was proposed for quadcopter attitude control to realize complex acrobatic manoeuvres. However successful PID controllers are commercially, they can't guarantee control system stability for various flight conditions with uncertainties and disturbances. In [6], a neural network was used to learn the complete dynamics of the multi-rotor and an output feedback control law is developed to control the translational and rotational motion of the vehicle. The authors in [7] proposed a $PI^\lambda D^\mu$ neural network aided finite impulse response control scheme for multi-rotor UAVs. In these and similar schemes, it is difficult to quantify whether the controller is near the limits to its performance in order to decide on a modified flight path or landing. Again, it is difficult to know how to use these controllers in realtime and onboard decision making on flight safety.

A number of robust control schemes have been developed to overcome the modelling uncertainty or disturbances of multi-rotor UAVs. In [8], a robust L_1 optimal control for a multi-rotor was presented and experimentally evaluated. The control objective was to follow the desired trajectory with rejecting persistent disturbances by minimizing the L_∞ gain of the plant for these disturbances. Another control method, based on a robust compensation, was proposed in [9] to minimize the effect of aerodynamic disturbances and variable mass distribution.

Several nonlinear control methodologies have been derived by algebraic manipulation in Lyapunov stability derivations. A variety of these is available in the literature. In [10], a nonlinear model-based cascaded controller was

proposed by identifying the dynamical parameters of a generic quadcopter. A disturbance based observer for hovering control was proposed in [11]. The authors conducted an extensive analysis of multi-rotor dynamics to provide guidelines for designing a robust control scheme. In [12], a hover mode control based on multi-loop back-stepping design is introduced for a linearized multi-rotor dynamics. An attitude stabilization controller, based on quaternion feedback and integrator backstepping was proposed in [13]. The controller ensures that all the system states are uniformly ultimately bounded with the existence of external disturbances. Similarly, a nonlinear backstepping-based control for multi-rotor aircraft was introduced in [14]. Control system stability was evaluated by Lyapunov methods and LaSalle's invariance theorem with the presence of external disturbances. Other backstepping-based control schemes of multi-rotors can be found in [15, 16, 17]. Sliding mode control has also been used for multi-rotor UAV control. In [18], an adaptive fuzzy gain-scheduling sliding mode controller is introduced for multi-rotor attitude control. The sliding mode controller is used to control the attitude of the aircraft in the presence of modelling uncertainness and disturbances while the fuzzy logic system is used to reduce the chattering problem produced by the sliding mode controller. In [19], a robust integral sliding mode controller is developed for attitude control to cope with the parametric uncertainty of quadcopters. A backstepping controller with sliding mode observer is proposed in [20] that overcomes the uncertainty and disturbances of the vehicle. A similar approach was conducted in [21] to reduce external disturbance and load variation effects. Dynamic inversion control has also been employed to control a quadcopter. In [22], a nonlinear dynamics inversion control scheme

4

is developed for a multi-rotor system to decouple the attitude and position dynamics and maximize the transmission bandwidth of position control by considering system uncertainty and disturbances. Similarly, a robust dynamic inversion approach is proposed in [23] for controlling and stabilizing under disturbances. A sensor-based incremental nonlinear dynamic inversion controller is developed in [24], with sliding mode disturbance observers for fault-tolerant control, in order to reduce the effects of model uncertainty and disturbances. Control of multi-rotor UAVs, which concern themselves by either modelling error or by flight disturbances, have been subject to various investigations [25, 26, 27].

Although there have been a variety of controllers proposed to control multi-rotors, most of the work available is either concerned with modelling uncertainty or with disturbances. Both *inertial matrix uncertainty and external disturbances* are important factors and can affect the craft at the same time in practice. The upper limits of these need to be known in order to be included in the design and to be known to onboard decisions affecting flight safety .

In this paper a control scheme for a generic multi-rotor is presented that consists of inner and outer loops, now common in aerospace. The inner loop is a robust nonlinear dynamic inversion (RNDI) attitude controller to deal with modelling uncertainty and external disturbances. It is developed based on the well-known dynamic inversion technique [28, 29]. The outer loop is a feedback position controller, which handles the vehicle lateral and vertical transitions. A Lyapunov method is used as part of the attitude controller design to ensure system stability. The novelty of this paper is

represented by introducing a new controller that is robust to both modelling errors and external disturbances, while it can monitor the violation of its stability condition as well.

2. Mathematical Model

This section introduces the dynamical model of a generic multi-rotor using quaternions to avoid the singularity associated with the gimbal lock [30], which is important in high-performance control.

2.1. Quaternions

Gimbal lock occurs due to possible singularity of the direct cosine matrix (DCM) in terms of Euler angles. To avoid gimbal lock, a quaternions representation [31, 32] can be used to define rigid body attitude. The unit quaternions are defined as

$$\boldsymbol{q} = [q_0 \quad \boldsymbol{q}_v^T]^T = [q_0 \ q_1 \ q_2 \ q_3]^T, \tag{1}$$

where $\boldsymbol{q} \in \Re^4$ is the quaternion, $q_0 \in \Re$ is its scalar element (cosine of a rotation angle), and $\boldsymbol{q}_v \in \Re^3$ is its vector element (aligned with the axis of rotation). The quaternion is suitable to describe any attitude of a rigid body by Euler's theorem, which states that two geometrically identical bodies can be transformed into each other by a parallel shift of one of the bodies and a single rotation around some axis in 3D space .There is the convention that for attitude we use unit quaternions such that $\|\boldsymbol{q}\| = \sqrt{q_0^2 + q_1^2 + q_2^2 + q_3^2} = 1$, hence $\boldsymbol{q}_v \in \Re^3$ is a unit vector multiplied by the sine of the rotation angle. Note that no-rotation (no attitude change) is not the zero quaternion but [1 0 0 0].

The transformation from Euler angles sequence (yaw ψ, pitch θ, roll ϕ) to quaternion can be described as [31]

$$
\begin{bmatrix} q_0 \\ q_1 \\ q_2 \\ q_3 \end{bmatrix} = \begin{bmatrix} cos(\frac{\phi}{2})cos(\frac{\theta}{2})cos(\frac{\psi}{2}) + sin(\frac{\phi}{2})sin(\frac{\theta}{2})sin(\frac{\psi}{2}) \\ -cos(\frac{\phi}{2})sin(\frac{\theta}{2})sin(\frac{\psi}{2}) + cos(\frac{\theta}{2})cos(\frac{\psi}{2})sin(\frac{\phi}{2}) \\ cos(\frac{\phi}{2})cos(\frac{\psi}{2})sin(\frac{\theta}{2}) + sin(\frac{\phi}{2})cos(\frac{\theta}{2})sin(\frac{\psi}{2}) \\ cos(\frac{\phi}{2})cos(\frac{\theta}{2})sin(\frac{\psi}{2}) - sin(\frac{\phi}{2})cos(\frac{\psi}{2})sin(\frac{\theta}{2}) \end{bmatrix}, \tag{2}
$$

while the transformation from quaternion to Euler angles

$$
\begin{bmatrix} \phi \\ \theta \\ \psi \end{bmatrix} = \begin{bmatrix} atan2(2q_2q_3 + 2q_0q_1, \ q_0{}^2 - q_1{}^2 - q_2{}^2 + q_3{}^2) \\ -asin(2q_1q_3 - 2q_0q_2) \\ atan2(2q_1q_2 + 2q_0q_3, \ q_0{}^2 + q_1{}^2 - q_2{}^2 - q_3{}^2) \end{bmatrix}. \tag{3}
$$

There is however no problem with relating the Euler angle rotation rates to quaternion rates. The relationship between the quaternion rates $\dot{\boldsymbol{q}} \in \Re^3$ and the angular velocities $\boldsymbol{\omega}(t) = [\omega_x(t) \ \omega_y(t) \ \omega_z(t)]^T \in \Re^3$ in the B-frame can be stated [31] as

$$
\boldsymbol{\omega} = \tilde{Z}\dot{\boldsymbol{q}} \ , \quad \begin{bmatrix} \omega_x \\ \omega_y \\ \omega_z \end{bmatrix} = 2 \begin{bmatrix} -q_1 & q_0 & q_3 & -q_2 \\ -q_2 & -q_3 & q_0 & q_1 \\ -q_3 & q_2 & -q_1 & q_0 \end{bmatrix} \begin{bmatrix} \dot{q}_0 \\ \dot{q}_1 \\ \dot{q}_2 \\ \dot{q}_3 \end{bmatrix}, \tag{4}
$$

and $\dot{\boldsymbol{q}} = \tilde{Z}^T\boldsymbol{\omega}$ where $\tilde{Z}^T = \tilde{Z}^{-1}$ is an orthogonal matrix. This is useful in control as solid state gyroscopes are available to measure ω_x, ω_y, ω_z, hence giving an opportunity to integrate the attitude changes in realtime.

The transformation from the body coordinates, B-frame for short, to the world (inertial) coordinates, W-frame for short, can be expressed using the

7

following matrix [31]

$$R_q = \begin{bmatrix} q_0^2 + q_1^2 - q_2^2 - q_3^2 & 2(q_1 q_2 - q_0 q_3) & 2(q_0 q_2 + q_1 q_3) \\ 2(q_1 q_2 + q_0 q_3) & q_0^2 - q_1^2 + q_2^2 - q_3^2 & 2(q_2 q_3 - q_0 q_1) \\ 2(q_1 q_3 - q_0 q_2) & 2(q_0 q_1 + q_2 q_3) & q_0^2 - q_1^2 - q_2^2 + q_3^2 \end{bmatrix}, \quad (5)$$

and from W-frame to B-frame using R_q^T where $R_q^T = R_q^{-1}$ is an orthogonal matrix of 3D rotations.

2.2. Multi Rotor Dynamic Model

The multi-rotor translational dynamics in the B-frame using a Newton equation is

$$m\dot{\boldsymbol{v}} + \Gamma(\boldsymbol{\omega})m\boldsymbol{v} = R_q^T \boldsymbol{f}_G + \boldsymbol{f}_B, \quad (6)$$

where $m \in \Re$ is the total mass of the craft, $\boldsymbol{v}(t) = [v_x(t)\ v_y(t)\ v_z(t)]^T \in \Re^3$ is the velocity vector of mass centre, $\dot{\boldsymbol{v}}(t) = [\dot{v}_x(t)\ \dot{v}_y(t)\ \dot{v}_z(t)]^T \in \Re^3$ is the acceleration vector, $\boldsymbol{f}_G = [0\ 0\ -mg]^T$ is the gravitational force, $\boldsymbol{f}_B = [0\ 0\ U]^T \in \Re^3$ is the total force of thrusters, $U = F_1 + F_2 + F_3 + F_4$, and $\Gamma(\boldsymbol{\omega}) \in \Re^{3\times3}$ is the cross-product matrix for the Coriolis forces such that $\boldsymbol{\omega} \times m\boldsymbol{v} = \Gamma(\boldsymbol{\omega})m\boldsymbol{v}$,

$$\Gamma(\boldsymbol{\omega}) = \begin{bmatrix} 0 & -\omega_z & \omega_y \\ \omega_z & 0 & -\omega_x \\ -\omega_y & \omega_x & 0 \end{bmatrix}. \quad (7)$$

The dynamics in the world frame $W = [X_W\ Y_W\ Z_W]^T$ will be

$$\ddot{\boldsymbol{r}} = \frac{1}{m}(\boldsymbol{f}_G + R_q \boldsymbol{f}_B), \quad (8)$$

where $\boldsymbol{r}(t) = [x(t)\ y(t)\ z(t)]^T \in \Re^3$ is the position vector in W-frame; since $\ddot{\boldsymbol{r}} = R_q \dot{\boldsymbol{v}}$. The multi-rotor rotational dynamics in the B-frame, using a

8
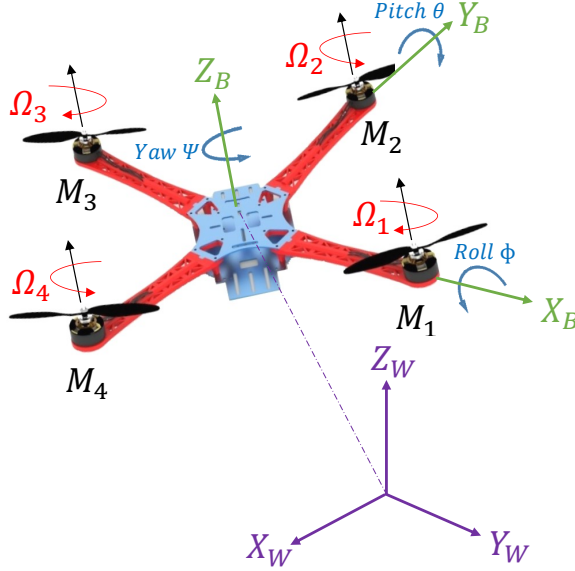
Figure 1: A quadcopter illustration in body frame and in inertia frames.

Newton-Euler equation, is

$$I\dot{\boldsymbol{\omega}} + \Gamma(\boldsymbol{\omega})I\boldsymbol{\omega} + \boldsymbol{\tau}_d = \boldsymbol{\tau}, \qquad (9)$$

where $I \in \Re^{3\times3}$ is the symmetric and positive-definite inertia matrix of the craft about its mass centre. $\boldsymbol{\tau}_d(t) = [\tau_{d\phi}(t)\ \tau_{d\theta}(t)\ \tau_{d\psi}(t)]^T \in \Re^3$ are the unknown disturbances torques with ϕ, θ and ψ are roll, pitch and yaw respectively. $\boldsymbol{\tau}(t) = [\tau_\phi(t)\ \tau_\theta(t)\ \tau_\psi(t)]^T \in \Re^3$ is the torque vector of the onboard controller in the B-frame which produces the multi-rotor motion.

We assume that for our multi-rotor each motor is aligned with the vertical main axis of the vehicle and has an angular velocity Ω_i that produces body-aligned forces $F_i = l\Omega_i^2$ and a torques $M_i = b\Omega_i^2$ with l and b are the aerodynamic force and torque constants of the rotors. All angular velocities of the motors are bounded by a known maximum value Ω_{max} so that,

9

$|\Omega_i| < \Omega_{max}$.

The torque output of the onboard control system, $\boldsymbol{\tau}$, for plus-configuration is

$$\boldsymbol{\tau} = \begin{bmatrix} \tau_\phi \\ \tau_\theta \\ \tau_\psi \end{bmatrix} = \begin{bmatrix} \ell l(\Omega_2^2 - \Omega_4^2) \\ \ell l(-\Omega_1^2 + \Omega_3^2) \\ b(-\Omega_1^2 + \Omega_2^2 - \Omega_3^2 + \Omega_4^2) \end{bmatrix}, \qquad (10)$$

where ℓ is the length from the centre of mass of the multi-rotor to the rotor. For an X-configuration, where propellers 1-2 are on the front, these equations are modified to

$$\boldsymbol{\tau} = \begin{bmatrix} \tau_\phi \\ \tau_\theta \\ \tau_\psi \end{bmatrix} = \begin{bmatrix} \ell l(-\Omega_1^2 + \Omega_2^2 + \Omega_3^2 - \Omega_4^2)/\sqrt{2} \\ \ell l(-\Omega_1^2 - \Omega_2^2 + \Omega_3^2 + \Omega_4^2)/\sqrt{2} \\ b(-\Omega_1^2 + \Omega_2^2 - \Omega_3^2 + \Omega_4^2) \end{bmatrix}, \qquad (11)$$

For a hexacopter one of the options is, where propellers 1-2 are on the front, to have the attitude control torques generated by

$$\boldsymbol{\tau} = \begin{bmatrix} \tau_\phi \\ \tau_\theta \\ \tau_\psi \end{bmatrix} = \begin{bmatrix} \ell l(-\Omega_1^2/2 + \Omega_2^2/2 + \Omega_3^2 + \Omega_4^2/2 - \Omega_5^2/2 - \Omega_6^2) \\ \ell l(-\Omega_1^2 - \Omega_2^2 + \Omega_4^2 + \Omega_5^2)\sqrt{3}/2 \\ b(-\Omega_1^2 + \Omega_2^2 - \Omega_3^2 + \Omega_4^2 - \Omega_5^2 + \Omega_6^2) \end{bmatrix}, \qquad (12)$$

The torques can be modelled in a similar manner for other types of multirotor configurations, which are out of the scope of this paper.

For all cases of multi-rotors, from Eq. (9), and denoting by $c(\boldsymbol{\omega}) = \Gamma(\boldsymbol{\omega})I\boldsymbol{\omega}$ the torque generated by the rotational moments, the attitude state-space equation derives from

$$\dot{\boldsymbol{\omega}} = I^{-1}[\boldsymbol{\tau} - \boldsymbol{c}(\boldsymbol{\omega}) - \boldsymbol{\tau}_d]. \qquad (13)$$

3. Control System Design

The nonlinear rotational dynamics, when combined with minor inaccuracies in rotor shaft alignments and propeller deficiencies can lead to errors in actuated control torques. The effect of these can be eliminated by an inner-loop feedback controller of the multi-rotor attitude. The same attitude controller can also be used to compensate for external disturbances of wind gusts, aerodynamic interactions with nearby structures and ground effects. Fig. 2 shows the proposed control system where the inner loop is embedded in an outer feedback loop to control lateral and vertical movements, which include pre-computing desired roll and pitch angles for manoeuvre-goals in the x, y, z lateral position frame.
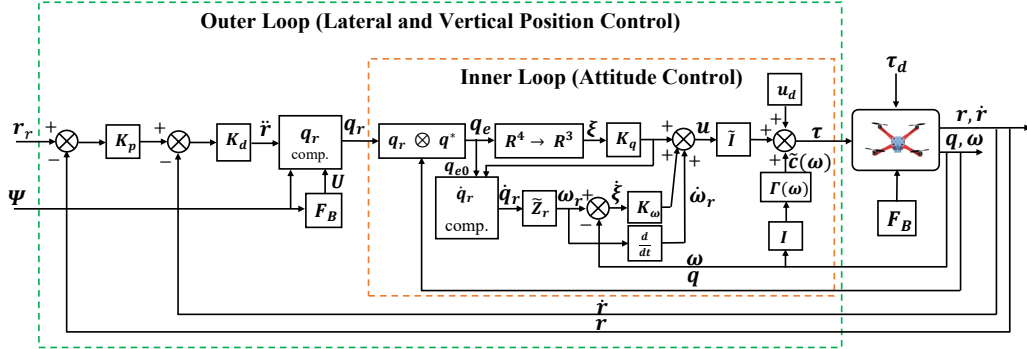
Figure 2: The inner and outer control loops of the proposed multi-rotor controller. The notation is explained through equations (16)-(30).

3.1. Position Control

Multi-rotor lateral transition is obtained by tilting the vehicle around X-axis by (q_0, q_1) and Y-axis by (q_0, q_2) for the quadrotor illustrated in Fig.1.

These angles are computed based on the reference trajectory of the position controller, which passes them to the inner attitude controller. However, the outer feedback position control loop is chosen as cascaded $P(x), P(y)$ controllers to handle the $\dot{x}$ and $\dot{y}$. Another cascaded $P(z)$ controller is also chosen to control $\dot{z}$ and hence obtaining the required linear movement.

Given the reference trajectory vector $\boldsymbol{r}_r(t) = [x_r(t)\ y_r(t)\ z_r(t)]^T \in \Re^3$ and $q_{r_3}(t)$ as in Eqs. (5) and (8) while keeping $\|\boldsymbol{q}\| = 1$, the quaternion reference $\boldsymbol{q}_r$ is computed by

$$\boldsymbol{q}_r = \begin{bmatrix} q_{r_0} \\ q_{r_1} \\ q_{r_2} \\ q_{r_3} \end{bmatrix} = \begin{bmatrix} [(\ddot{z}+g)/(2[\ddot{x}^2 + \ddot{y}^2 + \ddot{z}^2 + 2g\ddot{z} + g^2]^{\frac{1}{2}}) + 0.5 - q_{r_3}^2]^{\frac{1}{2}} \\ m(\ddot{x}q_{r_3} - \ddot{y}q_{r_0})/2U(q_{r_0}^2 + q_{r_3}^2) \\ m(\ddot{x}q_{r_0} + \ddot{y}q_{r_3})/2U(q_{r_0}^2 + q_{r_3}^2) \\ q_{r_3} \end{bmatrix}. \quad (14)$$

The force $\boldsymbol{f}_B$ including the total thrust U is computed for vehicle altitude control as

$$\boldsymbol{f}_B = \begin{bmatrix} 0 \\ 0 \\ U \end{bmatrix} = \begin{bmatrix} 0 \\ 0 \\ (m\ddot{z} + mg)/(2q_0^2 + 2q_3^2 - 1) \end{bmatrix}. \quad (15)$$

Definition 1. *The translational motion is controlled by choosing*

$$\ddot{\boldsymbol{r}} = K_d(K_p(\boldsymbol{r}_r - \boldsymbol{r}) - \dot{\boldsymbol{r}}), \quad (16)$$

or in terms of components

$$\ddot{\boldsymbol{r}} = \begin{bmatrix} \ddot{x} \\ \ddot{y} \\ \ddot{z} \end{bmatrix} = \begin{bmatrix} K_{dx}(K_{px}(x_r - x) - \dot{x}) \\ K_{dy}(K_{py}(y_r - y) - \dot{y}) \\ K_{dz}(K_{pz}(z_r - z) - \dot{z}) \end{bmatrix}, \quad (17)$$

where $K_p = diag[K_{px}\ K_{py}\ K_{pz}]^T \in \Re^{3\times3}$ and $K_d = diag[K_{dx}\ K_{dy}\ K_{dz}]^T \in \Re^{3\times3}$ are positive-definite diagonal gain matrices.

12

The controller represented in Eq. (16) is implemented using Eq. (14) to get the quaternion reference required for the multi-rotor attitude control and using Eq. (15) to compute the total amount of thrust, U.

3.2. Attitude Control

Our nonlinear control system is designed based on the dynamic inversion control principle [28], for controlling the multi-rotor attitude while accounting for the bounded but uncertain mass distribution of the aircraft and external force and torque disturbances. Lyapunov's method will be used to prove asymptotic stability under these bounded uncertainties for the control system defined as follows.

Definition 2. *Controller Torque Computation. Based on the attitude dynamics in Eq. (9), the nonlinear control law is defined by*

$$\boldsymbol{\tau} = \hat{I}\boldsymbol{u} + \boldsymbol{u}_d + \hat{\boldsymbol{c}}(\boldsymbol{\omega}), \tag{18}$$

Here $\hat{I}$ is an estimated matrix of the inertia matrix I of the craft, $\boldsymbol{u}$ represents a new input vector to be designed later on in Eq. (25), $\hat{\boldsymbol{c}}(\boldsymbol{\omega})$ is an estimate of $\boldsymbol{c}(\boldsymbol{\omega})$ as based on $\hat{I}$ and measured $\boldsymbol{\omega}$. The additional term $\boldsymbol{u}_d$ is added to render the effects of uncertainty and disturbances in addition to guarantee robustness of these effects; $\boldsymbol{u}_d$ will be defined later to counter these effects in Eq. (42).

Suppose that the attitude reference is $\boldsymbol{q}_r$ and the measured value is $\boldsymbol{q}$, the quaternion error $\boldsymbol{q}_e$ will be defined by

$$\boldsymbol{q}_e = \boldsymbol{q}_r \otimes \boldsymbol{q}^*, \tag{19}$$

13

where $\otimes$ is the Hamiltonian quaternion product and $\boldsymbol{q}^*$ denotes conjugate. Note that $\boldsymbol{q}^{-1} = \boldsymbol{q}^*$ as the attitude quaternion has norm 1. In algebraic detail, the quaternion error $\boldsymbol{q}_e$ is

$$\boldsymbol{q}_e = \begin{bmatrix} q_{e0} \\ q_{e1} \\ q_{e2} \\ q_{e3} \end{bmatrix} = \begin{bmatrix} q_{r0}q_0 + q_{r1}q_1 + q_{r2}q_2 + q_{r3}q_3 \\ -q_{r0}q_1 + q_{r1}q_0 + q_{r3}q_2 - q_{r2}q_3 \\ -q_{r0}q_2 + q_{r2}q_0 + q_{r1}q_3 - q_{r3}q_1 \\ -q_{r0}q_3 + q_{r3}q_0 + q_{r2}q_1 - q_{r1}q_2 \end{bmatrix}. \tag{20}$$

The tracking error vector will be defined as

$$\boldsymbol{\xi} = [q_{e_1} \; q_{e_2} \; q_{e_3}]^T, \tag{21}$$

since $\boldsymbol{\xi}$ is chosen to reduce the dimensions of $\mathbf{q}_e$ by neglecting q_{e0} that is near 1 for small attitude errors and is only indicative of the size of the rotation error. $\boldsymbol{\xi}$ will be used later in Eq. (25). Definition (21) can be justified on the grounds that $\boldsymbol{\xi}$ converges to zero when the attitudes of $\boldsymbol{q}$ and $\boldsymbol{q}_r$ converge, as then q_{e0} converges to 1 and $[q_{e_1} \; q_{e_2} \; q_{e_3}]^T$ converges component-wise to zero. For large rotational-error correction of attitude, we will define the desired reference quaternion rate $\dot{\boldsymbol{q}}_r$ based on the error $\boldsymbol{q}_e$ as

$$\dot{\boldsymbol{q}}_r = [k_{q0}q_{e0} \; [K_q\boldsymbol{\xi}]^T]^T, \tag{22}$$

where the scalar $k_{q0} > 0$ and $K_q = diag[k_{q1}k_{q2}k_{q3}] \in \Re^{3\times3}$ is a positive-definite diagonal gain matrix, and hence we account for large rotational errors through the rate reference. Note that the value of q_{e0} is not included in Eq. (21) but it is included in Eq. (22) to compute the reference quaternion rate.

Using the defined rate $\dot{\boldsymbol{q}}_r$ and the relation in Eq. (4), the error rate is can be derived as

$$\dot{\boldsymbol{\xi}} = \tilde{Z}_r\dot{\boldsymbol{q}}_r - \tilde{Z}\dot{\boldsymbol{q}} = \boldsymbol{\omega}_r - \boldsymbol{\omega}. \tag{23}$$

14

This choice of a reference rate $\dot{\boldsymbol{q}}_r$ will aid our proofs of control performance. Also note that $\dot{\boldsymbol{\omega}}_r$ can now be obtained from $\boldsymbol{\omega}_r$, as the latter can be made differentiable by a suitable choice of the desired attitude $\boldsymbol{q}_r$. For very small quaternion error, Eq. (23) can be simplified such that

$$\dot{\boldsymbol{\xi}} = \tilde{Z}_{q_e}\boldsymbol{\xi} = \mathbb{I}\,\boldsymbol{\xi} = \boldsymbol{\omega}_r - \boldsymbol{\omega}, \tag{24}$$

where $\mathbb{I}$ is identity 3×3 matrix. Note that Eq. (24) is only valid when the attitude error is small enough, i.e. q_e vector values with the maximum of $[1,\ 1.2350 * 10^{-5},\ 1.241 * 10^{-3},\ 0.850 * 10^{-7}]^T$.

Definition 3. *Controller Signal Computation. The control input $\boldsymbol{u}$ for Eq. (18) is defined by*

$$\boldsymbol{u} = \dot{\boldsymbol{\omega}}_r + K_{\boldsymbol{\omega}}\dot{\boldsymbol{\xi}} + K_{\boldsymbol{q}}\boldsymbol{\xi}, \tag{25}$$

where $K_\omega = diag[k_{\omega_1} k_{\omega_2} k_{\omega_3}] \in \Re^{3\times3}$ is a positive-definite diagonal gain matrix setting the error gains in feedback.

By substituting the control torque (18) into (13), the rotational dynamics in Eq. (13) becomes

$$\begin{aligned}
\dot{\boldsymbol{\omega}} &= I^{-1}\hat{I}\boldsymbol{u} + I^{-1}\boldsymbol{u}_d + I^{-1}[\boldsymbol{\Delta}(\boldsymbol{\omega}) - \boldsymbol{\tau}_d] \\
&= \boldsymbol{u} + (I^{-1}\hat{I} - \mathbb{I})\boldsymbol{u} + I^{-1}\boldsymbol{u}_d + I^{-1}[\boldsymbol{\Delta}(\boldsymbol{\omega}) - \boldsymbol{\tau}_d] \\
&= \boldsymbol{u} + I^{-1}\boldsymbol{u}_d - \boldsymbol{y}
\end{aligned} \tag{26}$$

where

$$\boldsymbol{y} = [\mathbb{I} - I^{-1}\hat{I}]\boldsymbol{u} - I^{-1}[\boldsymbol{\Delta}(\boldsymbol{\omega}) - \boldsymbol{\tau}_d] \ , \ \boldsymbol{\Delta}(\boldsymbol{\omega}) = \hat{\boldsymbol{c}}(\boldsymbol{\omega}) - \boldsymbol{c}(\boldsymbol{\omega}). \tag{27}$$

By Eqs. (21)-(26), it follows that we have the error dynamics as

$$\ddot{\boldsymbol{\xi}} + K_\omega\dot{\boldsymbol{\xi}} + K_q\boldsymbol{\xi} = \boldsymbol{y} - I^{-1}\boldsymbol{u}_d. \tag{28}$$

15

By setting $\boldsymbol{\eta} = [\boldsymbol{\xi} \ \dot{\boldsymbol{\xi}}]^T \in \Re^{6 \times 1}$, the closed-loop error dynamics equation is

$$\dot{\boldsymbol{\eta}} = A\boldsymbol{\eta} + G[\boldsymbol{y} - I^{-1}\boldsymbol{u}_d] \tag{29}$$

where

$$A = \begin{bmatrix} 0^{3 \times 3} & \mathbb{I}^{3 \times 3} \\ -K_q^{3 \times 3} & -K_\omega^{3 \times 3} \end{bmatrix}, \ G = \begin{bmatrix} 0^{3 \times 3} \\ \mathbb{I}^{3 \times 3} \end{bmatrix}. \tag{30}$$

To bound the error $\boldsymbol{\eta}$ we need to control the right-hand-side of Eq. (29) to be kept small and that will be achieved by definitions in Eq. (42) later. The new control input $\boldsymbol{u}$ need to guarantee asymptotic stability for any $\boldsymbol{y}$ varying within a bounded range. To ensure this, the following assumptions are made on the circumstances of the flight.

Assumption 1. (*Flight Envelop*): *As the motors have limited rotational rates, they have limited angular velocities $|\Omega_i| < \Omega_{max}$. The vehicle angular velocities $\|\boldsymbol{\omega}\| < \omega^{max}$ and angular accelerations $\|\dot{\boldsymbol{\omega}}\| < \dot{\omega}^{max}$ are also limited. It is assumed that a known upper bound $\alpha > 0$ limits the desired vehicle angular accelerations vector $\dot{\boldsymbol{\omega}}_r$ as*

$$\sup(\|\dot{\boldsymbol{\omega}}_r\|) < \alpha. \tag{31}$$

Assumption 2. (*Payload Characteristics*): *As the moments of inertia and mass of the vehicle may change with the payload to dangerous levels, they need to be constrained by limiting the amount of variation in the moments of inertia. The inertia matrix I is assumed to have a lower and upper bound, $\lambda_{min} > 0$, $\lambda_{max} > 0$, hence the requirement made is that*

$$\lambda_{min} \leq \|I^{-1}\| \leq \lambda_{max}. \tag{32}$$

Consequently, the deviation between the estimated matrix $\hat{I}$ and actual matrix I can also be described with some $\delta > 0$ in the format of

$$\|\mathbb{I} - I^{-1}\hat{I}\| \leq \delta \leq 1. \tag{33}$$

Assumption 3. *(**Weather and Aerodynamic Disturbances**): The external torque disturbance $\boldsymbol{\tau}_d$ is sufficiently smooth, due to mechanical inertia, and an upper constant bound $\gamma > 0$ is known so that*

$$\|\boldsymbol{\tau}_d\| \leq \gamma, \tag{34}$$

where $\gamma = \sup\ w(t)$; since $w(t)$ is the wind function that could violate the vehicle and its superior value can be estimated in practice.

Lemma 1. *Setting $\boldsymbol{\Delta}(\boldsymbol{\omega})$ as the error between the estimated vector $\hat{\boldsymbol{c}}(\boldsymbol{\omega})$ and the actual vector $\boldsymbol{c}(\boldsymbol{\omega})$, there exist $\beta > 0$ such that*

$$\|\boldsymbol{\Delta}(\boldsymbol{\omega})\| \leq \beta. \tag{35}$$

Proof. From $\boldsymbol{\Delta}(\boldsymbol{\omega}) = \hat{\boldsymbol{c}}(\boldsymbol{\omega}) - \boldsymbol{c}(\boldsymbol{\omega})$, $\hat{\boldsymbol{c}}_{\boldsymbol{\omega}} = \Gamma(\boldsymbol{\omega})\hat{I}\boldsymbol{\omega}$, and $\boldsymbol{c}(\boldsymbol{\omega}) = \Gamma(\boldsymbol{\omega})I\boldsymbol{\omega}$, we have

$$\begin{aligned} \boldsymbol{\Delta}(\boldsymbol{\omega}) &= \Gamma(\boldsymbol{\omega})\hat{I}\boldsymbol{\omega} - \Gamma(\boldsymbol{\omega})I\boldsymbol{\omega} \\ I^{-1}\boldsymbol{\Delta}(\boldsymbol{\omega}) &= -(\mathbb{I} - I^{-1}\hat{I})\Gamma(\boldsymbol{\omega})\boldsymbol{\omega}, \end{aligned} \tag{36}$$

by *Assumption* 1, where the upper limit of the angular acceleration is known, it is possible to compute the upper bound of the angular velocity, $\boldsymbol{\omega}$. Hence the angular velocity-dependent matrix, $\Gamma(\boldsymbol{\omega})$, is such that: $\sup(\|\boldsymbol{\omega}\|) \leq \sigma$ and $\sup(\|\Gamma(\boldsymbol{\omega})\|) \leq \varrho$ where $\sigma > 0$ and $\varrho > 0$; and using *Assumption* 2, we get

$$\begin{aligned} \|\boldsymbol{\Delta}(\boldsymbol{\omega})\| &\leq (\|\mathbb{I} - I^{-1}\hat{I}\|\ \|\Gamma(\boldsymbol{\omega})\|\ \|\boldsymbol{\omega}\|)/\|I^{-1}\| \\ &\leq (\delta\ \varrho\ \sigma)/\lambda_{max}\ := \beta. \end{aligned} \tag{37}$$

∎

3.3. Attitude Stability Analysis

The following theorem states the stability of the proposed controller based on Lyapunov's direct method, including the definition of the control term $\boldsymbol{u}_d$ in Eq. (18).

Theorem 1. *For the nonlinear dynamics in Eqs. (9), (25) using the control law in Eq. (18), the close-loop system is asymptotically stable and the control system's errors converge to zero with Assumptions 1-3.*

Proof. Setting the equilibrium point $\boldsymbol{\eta} = 0$ where $V(0) = 0$ and choosing the following positive-definite function

$$V(\boldsymbol{\eta}) = \boldsymbol{\eta}^T Q \boldsymbol{\eta} > 0 \ , \ \forall \boldsymbol{\eta} \neq 0 \tag{38}$$

where $Q \in \Re^{6 \times 6}$ is a symmetric positive-definite matrix, the time derivative of $V(\boldsymbol{\eta})$ in Eq.(38) along the trajectory of the system errors is

$$\begin{aligned} \dot{V}(\boldsymbol{\eta}) &= \dot{\boldsymbol{\eta}}^T Q \boldsymbol{\eta} + \boldsymbol{\eta}^T Q \dot{\boldsymbol{\eta}} \\ &= \boldsymbol{\eta}^T [A^T Q + QA] \boldsymbol{\eta} + 2 \boldsymbol{\eta}^T Q G(\boldsymbol{y} - I^{-1} \boldsymbol{u}_d), \end{aligned} \tag{39}$$

considering A has eigenvalues with all negative real parts, hence for a symmetric positive-definite matrix P, Lyapunov equation is written as

$$A^T Q + QA = -P. \tag{40}$$

This gives a unique solution Q then the term $\boldsymbol{\eta}^T [A^T Q + QA] \boldsymbol{\eta}$ in Eq. (39) is negative and the equation will be

$$\dot{V}(\eta) = -\boldsymbol{\eta}^T P \boldsymbol{\eta} + 2 \boldsymbol{\eta}^T Q G(\boldsymbol{y} - I^{-1} \boldsymbol{u}_d). \tag{41}$$

As the first term $-\boldsymbol{\eta}^T P \boldsymbol{\eta}$ is strictly negative, the second term $\boldsymbol{\eta}^T Q G(\boldsymbol{y} - I^{-1} \boldsymbol{u}_d)$ need also to be strictly negative to ensure $\dot{V}(\boldsymbol{\eta}) < 0$. Therefore, $\boldsymbol{u}_d$ must be chosen to render the second term.

18

Definition 4. *For a positive time-varying scalar function $\zeta(\boldsymbol{\eta}, t)$ which will be chosen to bound $\boldsymbol{y}$, the term $\boldsymbol{u}_d$ is defined as*

$$
\boldsymbol{u}_d = \begin{cases} \dfrac{\zeta(\boldsymbol{\eta}, t)}{\|G^T Q \boldsymbol{\eta}\|} G^T Q \boldsymbol{\eta}, & \text{if } \|G^T Q \boldsymbol{\eta}\| \geq \mu \\ \dfrac{\zeta(\boldsymbol{\eta}, t)}{\mu} G^T Q \boldsymbol{\eta}, & \text{if } \|G^T Q \boldsymbol{\eta}\| < \mu. \end{cases} \tag{42}
$$

The term $\boldsymbol{u}_d$ is defined as a continuous approximation of the discontinuous control because if $\boldsymbol{u}_d = \dfrac{\zeta(\boldsymbol{\eta}, t)}{\|G^T Q \boldsymbol{\eta}\|} G^T Q \boldsymbol{\eta}$ when $\|G^T Q \boldsymbol{\eta}\| \neq 0$ and $\boldsymbol{u}_d = 0$ at $\|G^T Q \boldsymbol{\eta}\| = 0$, a chattering problem will produce since $\boldsymbol{u}_d$ will be discontinuous which causes trajectories oscillation. To eliminate this problem, the error should vary within the boundary of μ if $\|G^T Q \boldsymbol{\eta}\|$ is less than this value. Note that $\boldsymbol{u}_d$ depends on the error $\boldsymbol{\eta}$ and with (42) bounded-norm error will be ensured.

Assuming that $\|G^T Q \boldsymbol{\eta}\| \geq \mu$, using Cauchy-Schwartz inequality we have

$$
\begin{aligned}
\boldsymbol{\eta}^T Q G (\boldsymbol{y} - I^{-1} \boldsymbol{u}_d) \leq & \|G^T Q \boldsymbol{\eta}\| \|\boldsymbol{y}\| - \lambda_{min} \zeta(\boldsymbol{\eta}, t) \|G^T Q \boldsymbol{\eta}\| \\
= & \|G^T Q \boldsymbol{\eta}\| (\|\boldsymbol{y}\| - \lambda_{min} \zeta(\boldsymbol{\eta}, t)),
\end{aligned} \tag{43}
$$

and if $\zeta(\boldsymbol{\eta}, t)$ is chosen such that the above term $\lambda_{min} \zeta(\boldsymbol{\eta}, t)$ is strictly positive and greater than $\|\boldsymbol{y}\|$, then $\dot{V}(\boldsymbol{\eta}) < 0$.

Definition 5. *If the term $\boldsymbol{y}$ is bounded such that $\|\boldsymbol{y}\| \leq \varepsilon$ for $\varepsilon > 0$, and for $\lambda_{min} > 0$, $\zeta(\boldsymbol{\eta}, t)$ can be chosen depending on $\boldsymbol{y}$ as*

$$
\zeta(\boldsymbol{\eta}, t) \geq \frac{\varepsilon}{\lambda_{min}}. \tag{44}
$$

From $\boldsymbol{y}$ in Eq. (27) and the *Assumptions* $1 - 3$ with Eq.(35), we get

$$
\begin{aligned}
\|\boldsymbol{y}\| \leq & \|\mathbb{I} - I^{-1} \hat{I}\| (\|\dot{\boldsymbol{\omega}}_r\| + \|K_\omega\| \|\dot{\boldsymbol{\xi}}\| + \|K_q\| \|\boldsymbol{\xi}\|) + \|I^{-1}\| (\|\boldsymbol{\Delta}(\boldsymbol{\omega})\| + \|\boldsymbol{\tau}_d\|) \\
\leq & \delta(\alpha + \|K_\omega\| \|\dot{\boldsymbol{\xi}}\| + \|K_q\| \|\boldsymbol{\xi}\|) + \lambda_{max}(\beta + \gamma) := \varepsilon,
\end{aligned} \tag{45}
$$

from the previous two equations, $\zeta(\boldsymbol{\eta}, t)$ obtained as

$$\zeta(\boldsymbol{\eta}, t) \geq \frac{\delta}{\lambda_{min}}(\alpha + \|K_\omega\|\|\dot{\boldsymbol{\xi}}\| + \|K_q\|\|\boldsymbol{\xi}\|) + \frac{\lambda_{max}}{\lambda_{min}}(\beta + \gamma). \qquad (46)$$

Finally, for $\|G^T Q\boldsymbol{\eta}\| \geq \mu$, Eq. (41) becomes

$$\dot{V}(\boldsymbol{\eta}) = -\boldsymbol{\eta}^T P\boldsymbol{\eta} + 2\boldsymbol{\eta}^T QG(\boldsymbol{y} - I^{-1}\frac{\zeta(\boldsymbol{\eta}, t)}{\|G^T Q\boldsymbol{\eta}\|}G^T Q\boldsymbol{\eta}) < 0, \qquad (47)$$

and for $\|G^T Q\boldsymbol{\eta}\| < \mu$,

$$\begin{aligned}
\boldsymbol{\eta}^T QG(\boldsymbol{y} - I^{-1}\boldsymbol{u}_d) &\leq \mu\|\boldsymbol{y}\| - \lambda_{min}\zeta(\boldsymbol{\eta}, t)\mu \\
&= \mu(\|\boldsymbol{y}\| - \lambda_{min}\zeta(\boldsymbol{\eta}, t)),
\end{aligned} \qquad (48)$$

then

$$\dot{V}(\boldsymbol{\eta}) = -\boldsymbol{\eta}^T P\boldsymbol{\eta} + 2\boldsymbol{\eta}^T QG(\boldsymbol{y} - I^{-1}\frac{\zeta(\boldsymbol{\eta}, t)}{\mu}G^T Q\boldsymbol{\eta}) < 0. \qquad (49)$$

∎

4. Simulation Studies

In order to test the controller performance in a realistic scenario, simulations have been carried out using the MathWorks team's detailed model [33] in Simulink/Matlab. The aircraft's nonlinear dynamics in (6) and (9) have been implemented in the model. The DC motors with propeller dynamics were also modelled based on parameters taken from real multi-rotor motor combinations. Moreover, the model has included computations of the motors' angular velocities Ω_{i_r} from the computed thrust U and torques $\boldsymbol{\tau}$ demanded by the control scheme. The computed Ω_{i_r} values had been applied to the motor and propeller dynamics and then realistic thrust U and torques $\boldsymbol{\tau}$ were obtained to approach the behaviour of a real dynamics. The original

20

MathWorks model has been modified with the use of quaternions instead of Euler angles, inertia moments variations, according to the payload change, were considered, disturbances were added to the torques. The proposed nonlinear controller has been compared to a nonlinear adaptive fractional order sliding mode based back-stepping (FRSDBKAD) controller presented in [21] in terms of robustness and stability and in this section reported.

4.1. Nominal Performance

The initial task is to track the desired position trajectory $\boldsymbol{r}_r = [x_r \; y_r \; z_r]^T$ and a desired rotation q_{3_r} without disturbances, where all the initial reference x_r, y_r, z_r, q_{3_r} are set to zero. Fig. 3 illustrates the desired trajectory of the drone which includes take-off, several manoeuvres and landing. According to the given trajectory, the RNDI controller shows that the measured x, y, z well followed the reference trajectory as can be seen in Fig. 3. The attitude controller results are shown in Fig. 4, where the attitude controller tracks the reference quaternions produced by the position controller. Note that the actual quaternion q is computed from the measured rates using the standard continuous solver *ode23* in simulation which is based on Bogacki-Shampine method with order three, four stages and adaptive step size. The actual quaternion is normalized to reduce error accumulation using the standard quaternion normalization algorithm in [31]. In nominal flight conditions, the aircraft tracked the reference trajectory well and more accurately than the FRSDBKAD controller.
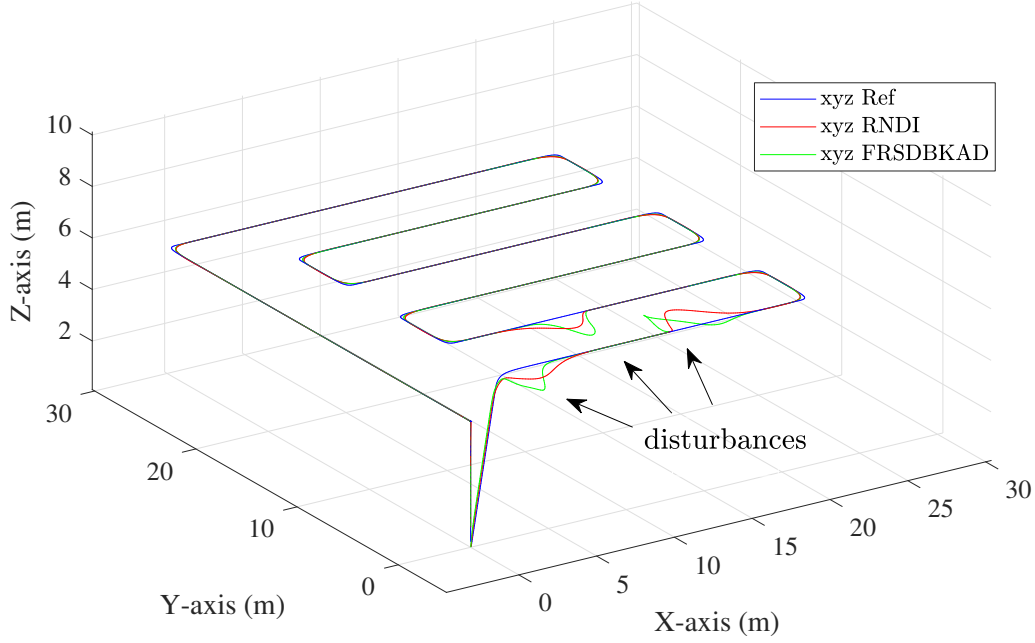
Figure 3: Three dimensional xyz trajectory in the W-frame. Ref: reference trajectory, RNDI: the proposed dynamic inverse controller, and FRSDBKAD: adaptive fractional order sliding mode based back-stepping controller. Differences can be seen under wind disturbances.

The controller parameters obtained are listed in Table 1. From Eq. (40), the positive definite diagonal matrix $P \in \Re^{6 \times 6}$ is chosen as

$$P = diag[9 * 10^{-12} \quad 9 * 10^{-12} \quad 5 * 10^{-13} \quad 3 * 10^{-10} \quad 3 * 10^{-10} \quad 8 * 10^{-10}], \quad (50)$$

and the symmetric positive definite matrix Q is obtained

$$Q = \begin{bmatrix} 1.566 * 10^{-11} & 0 & 0 & -4.5 * 10^{-12} & 0 & 0 \\ 0 & 1.566 * 10^{-11} & 0 & 0 & -4.5 * 10^{-12} & 0 \\ 0 & 0 & 2.539 * 10^{-9} & 0 & 0 & -2.5 * 10^{-13} \\ -4.5 * 10^{-12} & 0 & 0 & 2.466 * 10^{-10} & 0 & 0 \\ 0 & -4.5 * 10^{-12} & 0 & 0 & 2.466 * 10^{-10} & 0 \\ 0 & 0 & -2.5 * 10^{-13} & 0 & 0 & 6.347 * 10^{-8} \end{bmatrix}. \quad (51)$$

22
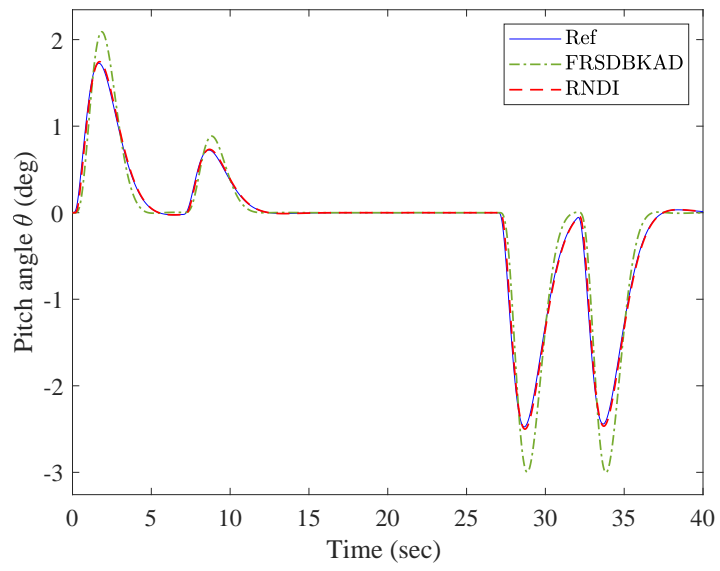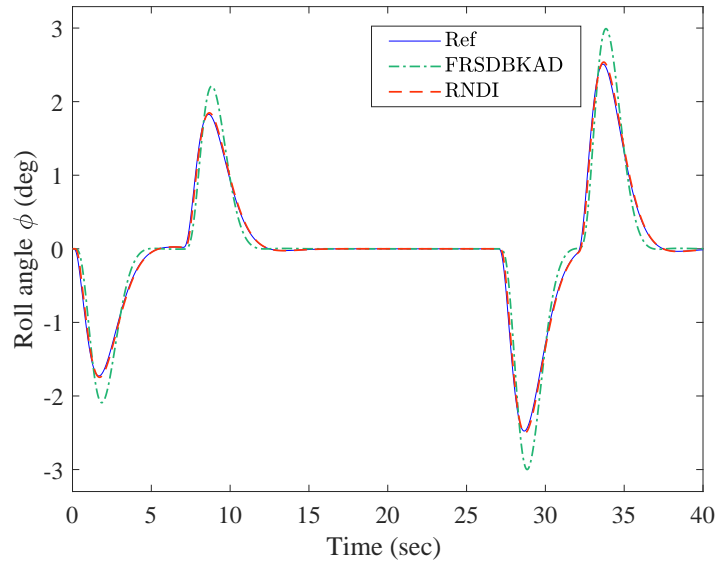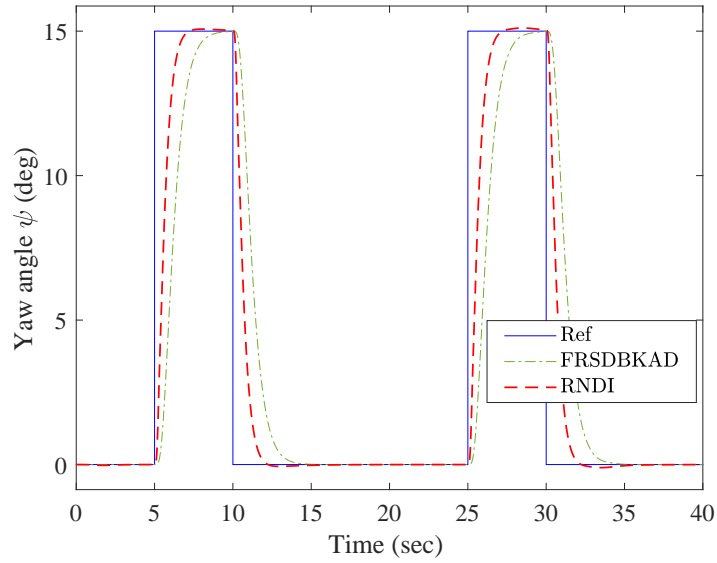
Figure 4: The measured angles track the reference attitude by adaptive fractional order sliding mode based back-stepping control (FRSDBKAD) and by robust nonlinear dynamics inversion (RNDI) control. The "*Roll angle* ϕ" shows the roll rotation around X-axis, "*Pitch angle* θ" shows the pitch rotation around Y-axis and "*Yaw angle* ψ" shows the yaw rotation around Z-axis; The blue continuous reference line almost coincides with the dashed RNDI controller proposed in this paper, while the dot-dashed FRSDBKAD controller is far from achieving that.

24

Table 1: Multi-rotor Parameters

Parameter	Value	Parameter	Value
$\hat{I}_x$	$5.831 * 10^{-3}\ kg.m^2$	b	$12 * 10^{-8}\ N.m/(rad/sec)^2$
$\hat{I}_y$	$5.831 * 10^{-3}\ kg.m^2$	l	$9 * 10^{-6}\ N/(rad/sec)^2$
$\hat{I}_z$	$1.166 * 10^{-2}\ kg.m^2$	α	180.7904
k_{q_0}	0.01	σ	36.3485
k_{q_1}	16	δ	0.04231
k_{q_2}	16	β	0.332
k_{q_3}	25	γ	0.4231
k_{ω_1}	0.9	μ	0.0095
k_{ω_2}	0.9	ϱ	36.3485
k_{ω_3}	0.0064	λ_{min}	171.045
ℓ	$0.2\ m$	λ_{max}	171.47
m	$0.9272\ kg$	Ω_{max}	$707.1068\ rad/sec$

4.2. Performance under Payload Uncertainties

The multi-rotor's flight controller should maintain the stability of the aircraft if its total mass changes due to adding payload, which causes a shift of its centre of gravity (CG) and changes the inertia matrix. In this subsection, we demonstrate this problem by testing our control scheme under a mass distribution change. Referring to *Assumption* 2, the maximum payload of the proposed multi-rotor has been set to 300 grams. Due to this mass distribution change, the moments of inertia will be altered. Considering the specified payload capacity that the multi-rotor can hold, the range of variation in the inertia moments is computed, hence the values of $\lambda_{min}, \lambda_{max}, \delta$ in Eqs. (32)

and (33) can be specified. By knowing these bounds, the proposed controller can compensate any variation of inertia moments within the specified range, where any change in inertia components is due to payload variation. These can even be inaccurate values of the inertia moments. Centre of the gravity error in modelling can be compensated by the proposed term u_d in Eq. (42) hence the aircraft will stay in the stable region.

The CG is computed by assuming the geometric CG is at the centre of the aircraft's hub, i.e. at point (0, 0, 0). Then the nominal diagonal inertia matrix components are computed. For any additional payload of up to 300 grams located within the hub of $10 \times 10 \times 4$ cm, for instance if the aircraft equipped with an omnidirectional camera or an arm to catch objects, the inertia matrix components (not diagonal) are computed for testing the controller with any payload change within the specified limits. Figure 5 illustrates the simulation test which is conducted to monitor the performance of the proposed control scheme when different payloads are applied. We have conducted this test by changing the aircraft's mass since different payloads were added to the aircraft's hub for up to 300 grams and consequently the CG and inertia moments were varied. The results show that the controller can cope well with any mass, CG and inertia matrix change within the specified bounds of $\lambda_{min}, \lambda_{max}$ and δ which have been formulated in *Assumption* 2.

However, to further increase the robustness of our control scheme for more reliable performance, a test can be executed before the flight to make an estimation of the range of uncertainty in terms of the payload changes, i.e. more accurate estimation of $\lambda_{min}, \lambda_{max}$, and δ. known methods such as in [34, 35, 36] can be used to estimate the inertia matrix while in flight and

disallow the flight if the $\lambda_{min}, \lambda_{max}, \delta$ are violated.

4.3. Performance under Aerodynamic Disturbances

This second illustration exposes the multi-rotor to some external torque disturbances to test the controller's behaviour and stability. External disturbances have been applied to the nominal torques and their effects on vehicle attitudes are illustrated in Fig. 6. We assumed that the disturbances are varying within 40% of the minimum/maximum torque $\boldsymbol{\tau}_{min/max} = [\pm 0.7446 \quad \pm 0.7446 \quad \pm 0.0993]^T$ Nm; where the range of disturbances for both roll and pitch is $\tau_{d\phi}, \tau_{d\theta} = [-0.2978, 0.2978]$ Nm and for yaw $\tau_{d\psi} = [-0.0397, 0.0397]$ Nm. The results in Fig. 6 illustrate how the controllers are reacting to the disturbances by counter acting the extra torques with some success in order to return the vehicle to follow the reference trajectory. The figures show the aircraft's attitudes in terms angles, where quaternions have been transferred to Euler angles using Eq. (3) for illustration. A comparison between FRSDBKAD control and our robust RNDI control is conducted to show how this controller is performing well, especially under high external disturbances for roll and pitch motion where the FRSDBKAD control performed less with some oscillations. The robust RNDI controller also does not hit the limits of the maximum actuator ($\Omega_{i\ max} = 707.1068$ rad/sec) even under high disturbances as can be seen from the measured angular velocities of the motors, Ω_i, in Fig. 7.

5. Discussion of Applicability

The ultimate aim of this work is to design a robust control scheme for multi-rotor UAVs that can provide a good or at least an acceptable per-
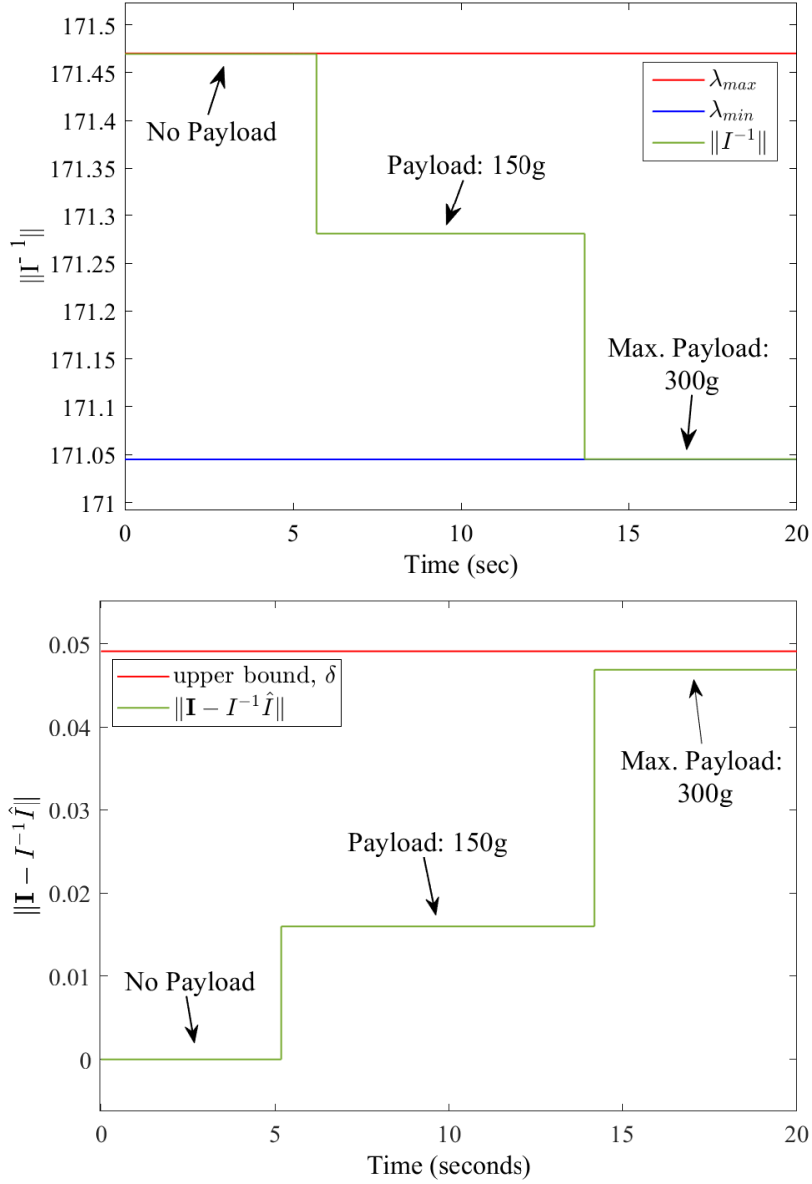
Figure 5: The first graph illustrates the norm of inertia matrix inverse $\|I^{-1}\|$ variation with payload change within the aircraft's hub ($Assumption$ 2 - Eq. (32)). The term $\|I^{-1}\|$ varies within the specified upper limit λ_{max} and lower limit λ_{min}. The second graph shows the effect of payload variation on the term $\|\mathbb{I} - I^{-1}\hat{I}\|$ which stays below the specified upper bound δ ($Assumption$ 2 - Eq. (33)).

28
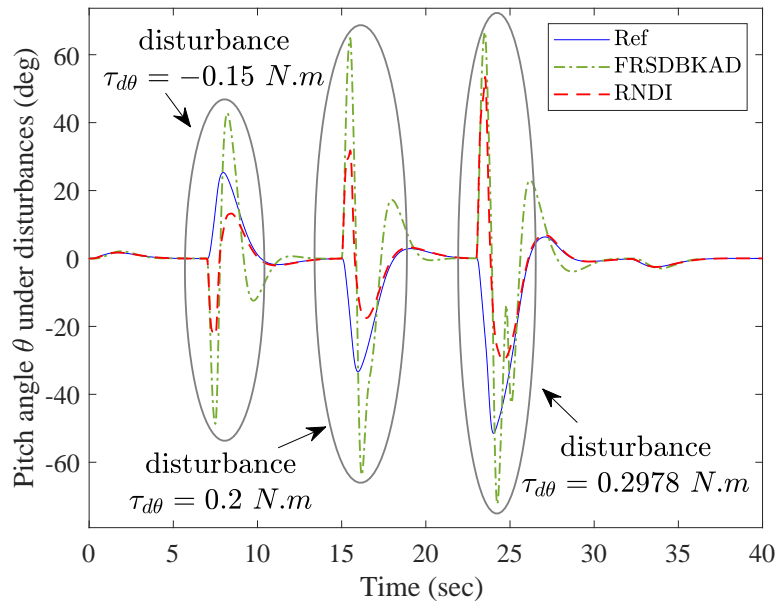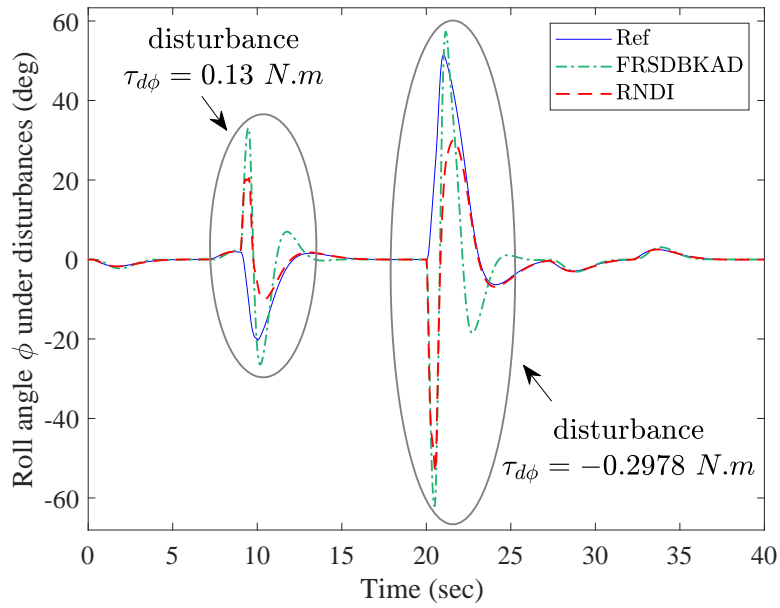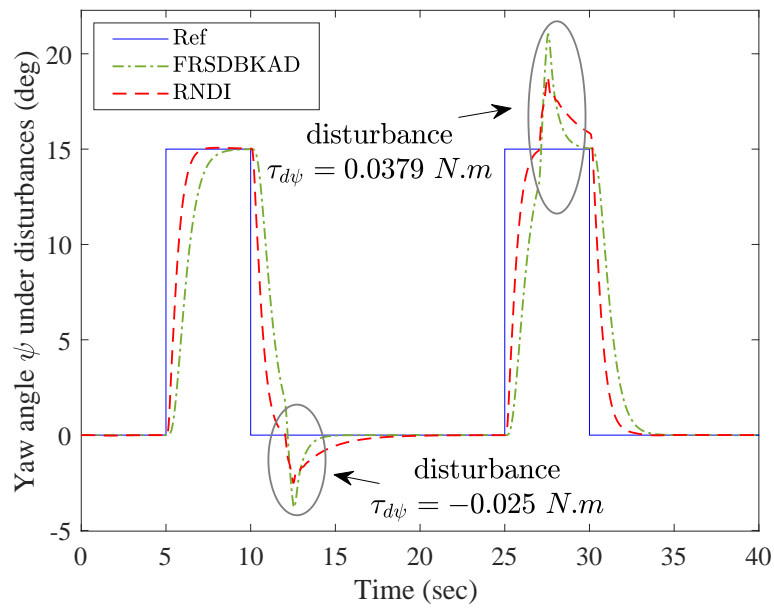
Figure 6: Attitudes under external disturbances show some oscillation in roll, ϕ, and pitch, θ, motion of the FRSDBKAD controller (dot-dashed green line) with less deviation in yaw, ψ, but not so for the RNDI (dashed red line) controller.
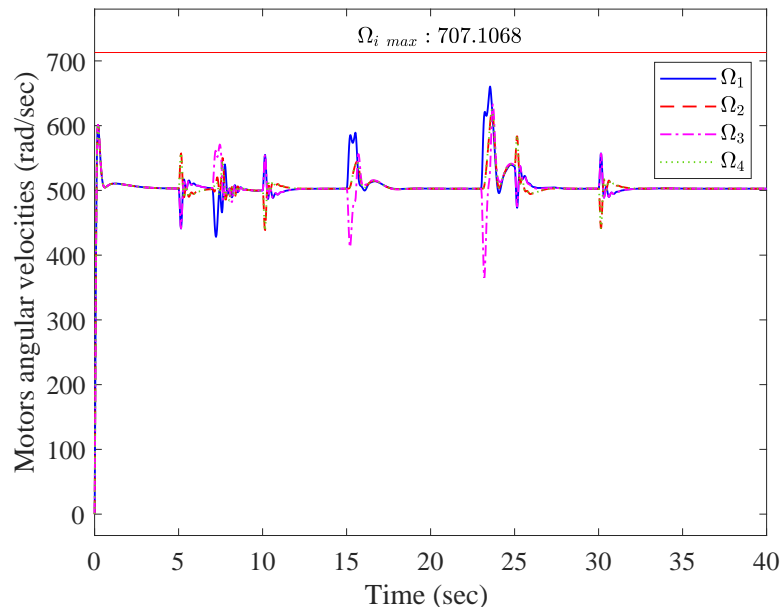
Figure 7: Actuators angular velocities computed from the RNDI control. It can be seen that the actuators limit, $\Omega_{i\ max}$, has not been reached even with the presence of disturbances.

formance and able to deal with different flight conditions such as payload change during the flight or when the vehicle is exposed to external forces, e.g. winds. These two conditions are very common in practice which may force the aircraft into unstable state-space regions, and as a consequence, the craft may crash and potentially cause damage to property, humans and privacy. However, in this paper we tackled these conditions in the modelling and design of a robust nonlinear controller for multi-rotor unmanned aircraft.

5.1. Environmental Conditions

The main two environmental conditions, which the aircraft may be exposed to, are the payload change and wind disturbances. The first considered condition, the payload variation, leads to a change in the mass of the aircraft, hence in its inertia moments can change. The range of these variations can be computed from the fact that the additional mass or payload is limited by the rotors lifting limits. Therefore, the aircraft should have a limited amount of payload that the actuators can handle. Knowing the possible range of vehicle's mass variations, one can set the lower and upper bounds of inertia moments as in Eqs. (32) and (33). This way any change in the payload within the specified range will produce stable control. For the second disturbance, wind disturbances, knowing the range of wind strengths, which the craft may be exposed to during its flight, leads to the design of a controller that accounts for additional torques that represent these disturbances for up to the maximum specified limit. The nonlinear term u_d defined in Eq. (42) compensates the variation of these conditions based on the specified bounds in Eqs. (32) and (34). Hence any variation in these two disturbances under specified bounds results in stable control of the aircraft. Note that u_d

32

is mainly defined based on the attitude errors under stability conditions to compensate for any external variation caused by winds or payload change.

In terms of inertia moment changes, which can be attributable to payload variation, the RNDI controller performs well by compensating the amount of moments change through the u_d term for any mass change that is within the specified limits as illustrated in Fig. 5. The RNDI controller has less deviation and oscillation in comparison with FRSDBKAD especially for roll and pitch for dealing with external wind disturbances as can be seen from Fig. 6. Keeping this deviation in attitude at the minimum will reduce the deviation from the reference trajectory, as can be seen in Fig. 3. It is also essential to avoid reaching the maximum motors' speed which has been considered in our control scheme as illustrated in Fig. 7 to preserve aircraft stability. Note that both payload change and wind disturbances have been applied at the same time to the aircraft in order to test the controller performance. The simulation results show that the RNDI controller can cope well even if both conditions occur within the specified limits stated in the proposed assumptions. This is a more realistic scenario that happens in practice and with this controller the aircraft can preserve its stability and tracking the given trajectory more effectively.

5.2. Multi-rotor UAVs Supported with Decision Making Strategies

The remaining question is how to address the situations when the maximum payload is reached or when the aircraft is exposed to extreme gusts of wind beyond the craft abilities, i.e. exceeding the maximum disturbance torques bounds considered during the control design. Answering these questions is essential for a safe and reliable flight of unmanned vehicles in general

and for autonomy in particular. Several studies have been conducted to provide the aircraft's autopilot with the ability to monitor its flight condition [37, 38, 39]. Other studies in [40, 41, 42, 43, 44, 45] have implemented intelligent agents supported by decision-making abilities to supervise the variations in the environmental conditions and to see whether they go beyond the specified limits then take the appropriate decisions.

The advantages of these studies can be exploited by providing the autopilot with a software agent, which is able to monitor whether the term u_d in $Definition$ 4 reaches its bounds or stay within the safe (stable) region. Another approach can be implemented by detecting out of bounds status by monitoring the limits of the actuators, i.e. observing the angular velocities of motors against their maximum boundaries ($\Omega_{i\ max}$); see Fig. 7. If these boundaries are reached for some period of time (can be tested and computed in practice), the agent can take the required decisions and perform emergency procedures to prevent incidents or reduce the risk of a crash. The agent may also inform the pilot or send warning messages to the nearest station to inform the need for an emergency landing, for instance. This approach increases flight safety and reduces the risk of collision or causing material damage.

Using the proposed RNDI control scheme under mild disturbances, the aircraft's autopilot does not need to estimate the inertia moments or wind disturbances on board as any variation of the conditions within the limits will be handled by the controller. When combined with inertia estimation and an onboard decision agent, high levels of robustness and safety can be achieved.

6. Conclusion

This paper has introduced a novel robust multi-rotor controller that accounts for both inertial uncertainty and disturbances. The proposed control system consists of two loops: an inner and outer loop. The inner loop is a nonlinear attitude controller, which is designed based on dynamic inversion control by taking into account dynamical uncertainty and external disturbances. The outer loop is a feedback position controller that computes the total thrust and reference quaternion values, which are passed to the inner loop. Lyapunov's second method is used as part of the control design to compute an additional nonlinear term that compensates for the uncertainty and disturbances and ultimately ensures stability under well-defined conditions in practice. The control system has been simulated based on a nonlinear multi-rotor model developed by MathWorks to test the control performance and it was compared with a competitive nonlinear controller. Ultimately, the paper's results may enhance the safety of multi-rotor unmanned aerial vehicles.

References

[1] H. Chao, Y. Cao, Y. Chen, Autopilots for small unmanned aerial vehicles: a survey, International Journal of Control, Automation and Systems 8 (1) (2010) 36–44.

[2] E. Capello, G. Guglieri, F. Quagliotti, D. Sartori, Design and validation of an $\mathcal{L}_1$ adaptive controller for mini-uav autopilot, Journal of Intelligent & Robotic Systems 69 (1-4) (2013) 109–118.

[3] J. Li, Y. Li, Dynamic analysis and PID control for a quadrotor, in: 2011 IEEE International Conference on Mechatronics and Automation, 2011, pp. 573–578. doi:10.1109/ICMA.2011.5985724.

[4] S. Fang, Y. Xu, J. Jiang, B. Hu, X. Que, The analysis on posture control of micro quadrotor based on PID, in: 2011 Fourth International Symposium on Computational Intelligence and Design, Vol. 2, 2011, pp. 283–286. doi:10.1109/ISCID.2011.173.

[5] Yun Yu, Shuo Yang, Mingxi Wang, Cheng Li, Zexiang Li, High performance full attitude control of a quadrotor on SO(3), in: 2015 IEEE International Conference on Robotics and Automation (ICRA), 2015, pp. 1698–1703. doi:10.1109/ICRA.2015.7139416.

[6] T. Dierks, S. Jagannathan, Output feedback control of a quadrotor UAV using neural networks, IEEE Transactions on Neural Networks 21 (1) (2010) 50–66. doi:10.1109/TNN.2009.2034145.

[7] M. Efe, Neural network assisted computationally simple $PI^\lambda D^\mu$ control of a quadrotor UAV, IEEE Transactions on Industrial Informatics 7 (2) (2011) 354–361. doi:10.1109/TII.2011.2123906.

[8] A. C. Satici, H. Poonawala, M. W. Spong, Robust optimal control of quadrotor UAVs, IEEE Access 1 (2013) 79–93.

[9] H. Liu, J. Xi, Y. Zhong, Robust motion control of quadrotors, Journal of the Franklin Institute 351 (12) (2014) 5494–5510.

[10] M. Beul, R. Worst, S. Behnke, Nonlinear model-based position control

for quadrotor UAVs, in: ISR/Robotik 2014; 41st International Symposium on Robotics, VDE, 2014, pp. 1–6.

[11] J. Kim, M.-S. Kang, S. Park, Accurate modeling and robust hovering control for a quad-rotor VTOL aircraft, in: Selected papers from the 2nd International Symposium on UAVs, Reno, Nevada, USA June 8–10, 2009, Springer, 2009, pp. 9–26.

[12] E. D. Vries, K. Subbarao, Backstepping based nested multi-loop control laws for a quadrotor, in: 2010 11th International Conference on Control Automation Robotics Vision, 2010, pp. 1911–1916. doi:10.1109/ICARCV.2010.5707890.

[13] X. Huo, M. Huo, H. R. Karimi, Attitude stabilization control of a quadrotor UAV by using backstepping approach, Mathematical Problems in Engineering 2014 (2014).

[14] X. Liang, Y. Fang, N. Sun, A novel nonlinear backstepping-based control approach for quadrotor unmanned aerial vehicle transportation systems, in: 2017 36th Chinese Control Conference (CCC), 2017, pp. 884–889. doi:10.23919/ChiCC.2017.8027457.

[15] Y. Yu, Y. Guo, X. Pan, C. Sun, Robust backstepping tracking control of uncertain MIMO nonlinear systems with application to quadrotor UAVs, in: 2015 IEEE International Conference on Information and Automation, 2015, pp. 2868–2873. doi:10.1109/ICInfA.2015.7279776.

[16] C. Fu, W. Hong, H. Lu, L. Zhang, X. Guo, Y. Tian, Adaptive robust backstepping attitude control for a multi-rotor unmanned aerial vehicle

with time-varying output constraints, Aerospace Science and Technology 78 (2018) 593–603.

[17] H. Ramirez-Rodriguez, V. Parra-Vega, A. Sanchez-Orta, O. Garcia-Salazar, Robust backstepping control based on integral sliding modes for tracking of quadrotors, Journal of Intelligent & Robotic Systems 73 (1-4) (2014) 51–66.

[18] Y. Yang, Y. Yan, Attitude regulation for unmanned quadrotors using adaptive fuzzy gain-scheduling sliding mode control, Aerospace Science and Technology 54 (2016) 208–217.

[19] C. T. Ton, W. MacKunis, Robust attitude tracking control of a quadrotor helicopter in the presence of uncertainty, in: 2012 IEEE 51st IEEE Conference on Decision and Control (CDC), 2012, pp. 937–942. doi:10.1109/CDC.2012.6426266.

[20] T. Madani, A. Benallegue, Sliding mode observer and backstepping control for a quadrotor unmanned aerial vehicles, in: 2007 American Control Conference, 2007, pp. 5887–5892. doi:10.1109/ACC.2007.4282548.

[21] M. Vahdanipour, M. Khodabandeh, Adaptive fractional order sliding mode control for a quadrotor with a varying load, Aerospace Science and Technology 86 (2019) 737–747.

[22] J. Wang, T. Bierling, M. Achtelik, L. Hocht, F. Holzapfel, W. Zhao, T. H. Go, Attitude free position control of a quadcopter using dynamic inversion, Infotech@Aerospace (2011). doi:10.2514/6.2011-1583.
URL https://arc.aiaa.org/doi/abs/10.2514/6.2011-1583

[23] A. Das, K. Subbarao, F. Lewis, Dynamic inversion with zero-dynamics stabilisation for quadrotor control, IET Control Theory & Applications 3 (3) (2009) 303–314.

[24] X. Wang, S. Sun, E.-J. van Kampen, Q. Chu, Quadrotor fault tolerant incremental sliding mode control driven by sliding mode disturbance observers, Aerospace Science and Technology (2019).

[25] E. L. de Angelis, F. Giulietti, G. Pipeleers, Two-time-scale control of a multirotor aircraft for suspended load transportation, Aerospace Science and Technology 84 (2019) 193–203.

[26] R. López-Gutiérrez, A. E. Rodriguez-Mata, S. Salazar, I. González-Hernández, R. Lozano, Robust quadrotor control: attitude and altitude real-time results, Journal of Intelligent & Robotic Systems 88 (2-4) (2017) 299–312.

[27] H. Liu, D. Derawi, J. Kim, Y. Zhong, Robust optimal attitude control of hexarotor robotic vehicles, Nonlinear dynamics 74 (4) (2013) 1155–1168.

[28] M. W. Spong, S. Hutchinson, M. Vidyasagar, Robot modeling and control, Vol. 3, Wiley New York, 2006.

[29] L. Sciavicco, B. Siciliano, Modelling and control of robot manipulators, Springer Science and Business Media, 2012. doi:10.1007/978-1-4471-0449-0.

[30] G. Vass, Avoiding gimbal lock, Comput. Graph. World 32 (6) (2009) 1011.

[31] B. L. Stevens, F. L. Lewis, E. N. Johnson, Aircraft control and simulation: dynamics, controls design, and autonomous systems, John Wiley and Sons, 2015.

[32] J. Diebel, Representing attitude: Euler angles, unit quaternions, and rotation vectors, Matrix 58 (15-16) (2006) 1–35.

[33] B. Horton, M. Australia, Modelling, simulation and control of a quadcopter, in: MATLAB Academic Conference. Australia and New Zealand, 2016, pp. 4–14, [Accessed: 26 July 2019].
URL https://uk.mathworks.com/videos/modelling-simulation-and-control-of-a-quadcopter-122872.html

[34] R. Lopéz, I. Gonzalez, J. Flores, J. Ordaz, S. Salazar, R. Lozano, Real time parameter identification of the inertia tensor for a quad-rotor mini-aircraft using adaptive control, IFAC Proceedings Volumes 46 (30) (2013) 32–37.

[35] M. Krznar, D. Kotarski, P. Piljek, D. Pavković, On-line inertia measurement of unmanned aerial vehicles using on board sensors and bifilar pendulum, Interdisciplinary Description of Complex Systems: INDECS 16 (1) (2018) 149–161.

[36] S. Yang, S. Lee, J.-H. Lee, H.-S. Oh, New real-time estimation method for inertia properties of STSAT-3 using gyro data, Transactions of the Japan Society for Aeronautical and Space Sciences 58 (4) (2015) 247–249.

[37] P. Doherty, J. Kvarnström, F. Heintz, A temporal logic-based planning and execution monitoring framework for unmanned aircraft systems, Autonomous Agents and Multi-Agent Systems 19 (3) (2009) 332–377.

[38] M. Vierhauser, J. Cleland-Huang, S. Bayley, T. Krismayer, R. Rabiser, P. Grünbacher, Monitoring CPS at runtime- a case study in the UAV domain, in: 2018 44th Euromicro Conference on Software Engineering and Advanced Applications (SEAA), IEEE, 2018, pp. 73–80.

[39] D. Wolfram, F. Vogel, D. Stauder, Condition monitoring for flight performance estimation of small multirotor unmanned aerial vehicles, in: 2018 IEEE Aerospace Conference, 2018, pp. 1–17. doi:10.1109/AERO.2018.8396471.

[40] S. Armanini, M. Polak, J. E. Gautrey, A. Lucas, J. F. Whidborne, Decision-making for unmanned aerial vehicle operation in icing conditions, CEAS Aeronautical Journal 7 (4) (2016) 663–675.

[41] J. Boubeta-Puig, E. Moguel, F. Snchez-Figueroa, J. Hernndez, J. Carlos Preciado, An autonomous UAV architecture for remote sensing and intelligent decision-making, IEEE Internet Computing 22 (3) (2018) 6–15. doi:10.1109/MIC.2018.032501511.

[42] S. Tantrairatn, S. M. Veres, A rational agent framework for adaptive flight control of UAVs, in: 2015 International Conference on Unmanned Aircraft Systems (ICUAS), IEEE, 2015, pp. 147–156.

[43] A. G. Shem, T. A. Mazzuchi, S. Sarkani, Addressing uncertainty in UAV

navigation decision-making, IEEE Transactions on Aerospace and Electronic Systems 44 (1) (2008) 295–313. doi:10.1109/TAES.2008.4517005.

[44] R. Evertsz, J. Thangarajah, N. Yadav, T. Ly, A framework for modelling tactical decision-making in autonomous systems, Journal of Systems and Software 110 (2015) 222–238.

[45] J. J. Ruz, O. Arevalo, G. Pajares, J. M. de la Cruz, Decision making among alternative routes for UAVs in dynamic environments, in: 2007 IEEE Conference on Emerging Technologies and Factory Automation (EFTA 2007), 2007, pp. 997–1004. doi:10.1109/EFTA.2007.4416892.